



This is a repository copy of *Assessment of the influence of lung inflation state on the quantitative parameters derived from hyperpolarized gas lung ventilation MRI in healthy volunteers.*

White Rose Research Online URL for this paper:  
<http://eprints.whiterose.ac.uk/138805/>

Version: Accepted Version

---

**Article:**

Hughes, P.J.C., Smith, L. [orcid.org/0000-0002-5769-423X](https://orcid.org/0000-0002-5769-423X), Chan, H.-F. [orcid.org/0000-0002-5382-2097](https://orcid.org/0000-0002-5382-2097) et al. (6 more authors) (2018) Assessment of the influence of lung inflation state on the quantitative parameters derived from hyperpolarized gas lung ventilation MRI in healthy volunteers. *Journal of Applied Physiology*. ISSN 8750-7587

<https://doi.org/10.1152/japplphysiol.00464.2018>

---

© 2018 American Physiological Society. This is an author produced version of a paper subsequently published in *Journal of Applied Physiology*. Uploaded in accordance with the publisher's self-archiving policy.

**Reuse**

Items deposited in White Rose Research Online are protected by copyright, with all rights reserved unless indicated otherwise. They may be downloaded and/or printed for private study, or other acts as permitted by national copyright laws. The publisher or other rights holders may allow further reproduction and re-use of the full text version. This is indicated by the licence information on the White Rose Research Online record for the item.

**Takedown**

If you consider content in White Rose Research Online to be in breach of UK law, please notify us by emailing [eprints@whiterose.ac.uk](mailto:eprints@whiterose.ac.uk) including the URL of the record and the reason for the withdrawal request.



[eprints@whiterose.ac.uk](mailto:eprints@whiterose.ac.uk)  
<https://eprints.whiterose.ac.uk/>

1 **Title:** Assessment of the influence of lung inflation state on the quantitative  
2 parameters derived from hyperpolarized gas lung ventilation MRI in healthy  
3 volunteers

4 **Authors:** Paul J.C. Hughes<sup>1</sup>, Laurie Smith<sup>1,2</sup>, Ho-Fung Chan<sup>1</sup>, Bilal A. Tahir<sup>1,3</sup>,  
5 Graham Norquay<sup>1</sup>, Guilhem J. Collier<sup>1</sup>, Alberto Biancardi<sup>1,4</sup>, Helen Marshall<sup>1</sup> and Jim  
6 M. Wild<sup>1</sup>

7 <sup>1</sup>POLARIS, Academic Unit of Radiology, University of Sheffield, Sheffield, South  
8 Yorkshire, United Kingdom; <sup>2</sup>Sheffield Children's Hospital, Sheffield, UK;  
9 <sup>3</sup>Academic Unit of Clinical Oncology, University of Sheffield, Sheffield, South  
10 Yorkshire, UK; <sup>4</sup>Insigneo Institute for in silico Medicine, University of Sheffield,  
11 Sheffield, UK

12 **Author contributions:**

13 Paul J.C. Hughes: Conceived and designed research, performed experiments,  
14 analyzed data, interpreted results of experiments, prepared figures, drafted manuscript,  
15 edited and revised manuscript, approved final version of manuscript

16 Laurie Smith: Performed experiments, edited and revised manuscript, approved final  
17 version of manuscript

18 Bilal A. Tahir: Analyzed data, edited and revised manuscript, approved final version  
19 of manuscript

20 Ho-Fung Chan: Performed experiments, edited and revised manuscript, approved  
21 final version of manuscript

22 Graham Norquay: Performed experiments, edited and revised manuscript, approved  
23 final version of manuscript

24 Guilhem J. Collier: Performed experiments, edited and revised manuscript, approved  
25 final version of manuscript

26 Alberto Biancardi: edited and revised manuscript, approved final version of  
27 manuscript

28 Helen Marshall: Interpreted results of experiments, edited and revised manuscript,  
29 approved final version of manuscript

30 Jim M. Wild: Conceived and designed research, interpreted results of experiments,  
31 edited and revised manuscript, approved final version of manuscript

32 **Corresponding Author:** Professor Jim M. Wild, PhD, Academic Unit of Radiology,  
33 Department of Infection Immunity and Cardiovascular Disease, University of  
34 Sheffield; Floor C, Royal Hallamshire Hospital, S10 2JF; + 44 (0)114 2159141;  
35 [j.m.wild@sheffield.ac.uk](mailto:j.m.wild@sheffield.ac.uk)

36 **Running head:** Multiple lung inflation level imaging using HP gas MRI

37

38 **ABSTRACT:** In this study, the effect of lung volume on quantitative measures of  
39 lung ventilation was investigated using MRI with hyperpolarized  $^3\text{He}$  and  $^{129}\text{Xe}$ . Six  
40 volunteers were imaged with hyperpolarized  $^3\text{He}$  at five different lung volumes  
41 (residual volume (RV), RV+1L, functional residual capacity (FRC), FRC+1L and  
42 total lung capacity (TLC)), and three were also imaged with hyperpolarized  $^{129}\text{Xe}$ .  
43 Imaging at each of the lung volumes was repeated twice on the same day with  
44 corresponding  $^1\text{H}$  lung anatomical images. Percentage lung ventilated volume (%VV)  
45 and variation of signal intensity (heterogeneity score,  $H_{\text{score}}$ ) were evaluated.  
46 Increased ventilation heterogeneity, quantified by reduced %VV and increased  $H_{\text{score}}$ ,  
47 was observed at lower lung volumes with the least ventilation heterogeneity observed  
48 at TLC. For  $^3\text{He}$  MRI data, the coefficient of variation of %VV was less than 1.5%  
49 and less than 5.5% for  $H_{\text{score}}$  at all lung volumes, whilst for  $^{129}\text{Xe}$  data the values were  
50 4% and 10% respectively. Generally, %VV generated from  $^{129}\text{Xe}$  images was lower  
51 than that seen from  $^3\text{He}$  images. The good repeatability of  $^3\text{He}$  %VV found here  
52 supports prior publications showing that percentage lung ventilated volume is a robust  
53 method for assessing global lung ventilation. The greater ventilation heterogeneity  
54 observed at lower lung volumes indicates that there may be partial airway closure in  
55 healthy lungs and that lung volume should be carefully considered for reliable  
56 longitudinal measurements of %VV and  $H_{\text{score}}$ . The results suggest that imaging  
57 patients at different lung volumes may help to elucidate obstructive disease  
58 pathophysiology and progression.

59

60 **KEYWORDS:** Imaging; MRI; Hyperpolarized gas; Lungs; Inflation;

61

62

63 **NEW AND NOTEWORTHY:** We present repeatability data of quantitative metrics  
64 of lung function derived from hyperpolarized helium-3, xenon-129 and proton  
65 anatomical images acquired at five lung volumes in volunteers. Increased regional  
66 ventilation heterogeneity at lower lung inflation levels was observed in the lungs of  
67 healthy volunteers.

68

69 ABSTRACT WORD COUNT: 246/250

70 NEW AND NOTEWORTHY WORD COUNT: 43/75

71 MANUSCRIPT WORD COUNT:

72 FIGURE COUNT: 9

73 TABLE COUNT: 7

74

## 75 **Introduction**

76 Hyperpolarized (HP) gas ventilation-weighted magnetic resonance imaging (MRI)  
77 allows the visualization of gas distribution within the lung and has been shown to  
78 detect early lung disease in patients with cystic fibrosis and normal spirometry (4, 19)  
79 and in the lungs of smokers (33). Additionally, it has been used to assess the response  
80 to treatment in patients with asthma (13, 29), to longitudinally assess patients with  
81 chronic obstructive pulmonary disease (17) and has been shown to be clinically  
82 feasible for assessing lung function in children (1).

83

84 HP gas and proton anatomical ( $^1\text{H}$ ) lung magnetic resonance imaging (MRI) can be  
85 combined to quantify lung ventilation using percentage lung ventilated volume  
86 (%VV) or its counterpart the ventilation defect percentage (%VDP) (33), both of  
87 which have been widely adopted as simple and robust image-derived metrics. %VV is  
88 the ratio of the ventilated lung, defined from HP gas ventilation-weighted images to  
89 the thoracic cavity volume, defined from the  $^1\text{H}$  anatomical images (16, 33). Previous  
90 work has shown improved repeatability of %VV when the anatomical image is  
91 acquired in the same breath-hold as the HP gas ventilation-weighted image (12).

92

93 Ventilation heterogeneity may be assessed by using the  $H_{\text{score}}$  metric developed by  
94 Tzeng et al. (31), which calculates the variation of signal intensity in a kernel around  
95 a given voxel as the standard deviation divided by the mean (e.g. Figure 1) (23, 31).

96

97 The clinical standard for assessing lung volumes is body plethysmography (22, 32),  
98 whilst changes in forced expiratory volume in one second ( $\text{FEV}_1$ ) and forced vital  
99 capacity, measured using spirometry, are used as clinical markers for lung function

100 decline in certain diseases (22, 32). However, patient coaching of inhalation from a  
101 bag of gas rather than spirometric gating is generally used to achieve the lung  
102 volumes for HP gas MR imaging, which may lead to variability in lung volumes as  
103 will the ability of the patient to inhale the entire contents of the bag of gas being used.  
104 The most frequently used lung volume is functional residual capacity plus 1 liter  
105 (FRC+1L) (6-8, 16, 18, 27, 34). However, if a 1L bag is inhaled from FRC in smaller  
106 patients this volume may be close to total lung capacity (TLC) and thus understanding  
107 the effect of lung inflation level on these image-derived metrics is important.

108

109 Previous work by Muradyan et al. (23) analyzed the effect of inhalation of HP xenon-  
110  $^{129}\text{Xe}$  from residual volume (RV) in healthy volunteers and sub-RV in elite  
111 divers by acquiring coronal projection images with an in-plane resolution of 4.7mm x  
112 9.4mm. Muradyan et al. calculated the global  $H_{\text{score}}$  in the ventilated regions of the  
113 image, and found that when the elite divers inhaled low volumes of gas (0.9L and  
114 0.4L respectively) compared to larger volumes of gas (1.3L and 0.9L respectively)  
115 from sub-RV, increased heterogeneity was seen in the images, consistent with  
116 punctate reopening of some airways that were closed at sub-RV. Marshall et al. (20)  
117 carried out preliminary work demonstrating the effect of airway opening between  
118 FRC+1L and TLC using HP  $^3\text{He}$  imaging showing decreased heterogeneity and  
119 increased %VV at TLC when compared to FRC+1L. With these studies  
120 demonstrating important mechanisms at work in healthy controls and patients it is  
121 clear that understanding the effect of lung inflation on quantitative metrics derived  
122 from HP gas and  $^1\text{H}$  anatomical MRI is an important step in moving these techniques  
123 forward into standard clinical practice.

124

125 Historically, noble gas MRI studies have made use of HP helium-3 ( $^3\text{He}$ ); however,  
126 with the rising cost and scarcity of  $^3\text{He}$ , the focus of the pulmonary imaging  
127 community is switching to the use of HP  $^{129}\text{Xe}$  (18, 27) where differences in metrics  
128 have been reported due to the differences in diffusivity and the achievable signal of  
129  $^{129}\text{Xe}$  MRI. Thus the aims of this study were to use both HP  $^3\text{He}$  and  $^{129}\text{Xe}$  MRI to:

- 130 1. assess the effect of different lung inflation levels on the HP gas image derived  
131 metrics %VV and  $H_{\text{score}}$ .
- 132 2. assess the repeatability of %VV and  $H_{\text{score}}$  from two same-day imaging  
133 sessions.

134

## 135 **Materials and methods**

### 136 Subjects

137 The study was performed with national research ethics committee approval and with  
138 informed consent from all volunteers. Six volunteers (all male) were recruited for this  
139 study with the only criterion being that subjects were suitable for MRI and had no  
140 known respiratory complications. Two volunteers were former smokers, two were  
141 occasional smokers and two were never smokers. Table 1 shows the subject  
142 demographics.

143

### 144 Study protocol

145 Spirometry was performed to international standards (32) to ensure subjects had were  
146 defined as spirometrically free from respiratory conditions.

147



148 All  $^3\text{He}$  imaging was carried out on a GE HDx 1.5T MRI scanner (GE Healthcare,  
149 Milwaukee, WI, USA) using a  $^3\text{He}$  transmit-receive flexible chest coil (Clinical MR  
150 Solutions, Brookfield, WI, USA).  $^3\text{He}$  was polarized using a commercial polarizer  
151 (GE Healthcare, Amersham, UK). HP  $^3\text{He}$  3D balanced steady state free precession  
152 and  $^1\text{H}$  spoiled gradient echo images were acquired in the same breath (12) at five  
153 different lung volumes: RV, RV+1L, FRC, FRC+1L and TLC. For  $^{129}\text{Xe}$  imaging, the  
154 gas was polarized using a home-built polarizer (24) and images were acquired using a  
155  $^{129}\text{Xe}$  transmit-receive flexible vest coil (Clinical MR Solutions, Brookfield, WI,  
156 USA) and the  $^1\text{H}$  system body coil at five different lung volumes, as with  $^3\text{He}$   
157 imaging.  $^{129}\text{Xe}$  and  $^1\text{H}$  images were acquired in separate breath-holds as previously  
158 described (27, 28) and this was due to the longer acquisition time of the  $^{129}\text{Xe}$  scan.  
159 Note that only a subset of the volunteers (V2, V3 and V6) were scanned using HP  
160  $^{129}\text{Xe}$  and separate-breath  $^1\text{H}$  imaging as a feasibility study as some participants were  
161 no longer available to be scanned. A 1L mixture of hyperpolarized gas and nitrogen  
162 was used as it is the most commonly used volume in adults (6-8, 16, 18, 27, 34).

163

164 For the breathing maneuvers (Figure 2), volunteers were coached and instructed to  
165 breathe within the scanner by a pulmonary physiologist. During imaging, breathing  
166 maneuvers started with inhalation of the contents of the 1L bag from FRC, except for  
167 imaging at RV+1L where volunteers first exhaled to RV. To acquire images at TLC,  
168 volunteers inhaled room air to maximum lung capacity after the inhalation of 1L of  
169 gas from the bag. For imaging at FRC, volunteers inhaled the contents of the 1L bag  
170 from FRC and then exhaled back to FRC. For RV imaging, volunteers inhaled the  
171 contents of the 1L bag from FRC and then exhaled to RV. Gas doses were increased  
172 for the exhalation maneuvers and for imaging at TLC with the aim of ensuring

173 sufficient signal for imaging, and prior to exhalation participants held their breath for  
174 5 seconds to allow the gas to diffuse into the peripheral lung. Inhaled gas doses are  
175 given in Table 2; note that images were also acquired in the order presented in Table  
176 2.

177

178 For  $^3\text{He}$  acquisitions, subjects were scanned twice on the same day, with a 10 to 20-  
179 minute break (remaining supine within the scanner) in between imaging sessions.  $^3\text{He}$   
180 imaging sessions lasted 20-30 minutes on average. For  $^{129}\text{Xe}$  imaging, subjects were  
181 scanned twice on the same day, with a 20 to 40-minute break between imaging  
182 sessions and were removed from the scanner during this break.  $^{129}\text{Xe}$  imaging  
183 sessions lasted 35-45 minutes on average, due to limitations imposed by gas  
184 polarization time.

185

#### 186 Image analysis

187 Thoracic cavity volume (TCV) and ventilated volume (VV) were extracted from the  
188  $^1\text{H}$  anatomical and HP gas ventilation images, respectively, using the semi-automated  
189 segmentation method based on spatial Fuzzy C-means thresholding previously  
190 described (15). Percentage lung ventilated volume was calculated according to  
191  $\%VV = (VV/TCV) \times 100$ .

192

193 Ventilation heterogeneity was assessed using a modified version of the  $H_{\text{score}}$  method  
194 previously described (31). Images were subsampled from 256x256 voxels in-plane to  
195 128x128 voxels, resulting in an apparent image resolution of  $\sim 3.2 \times 3.2 \times 5\text{mm}$  for  $^3\text{He}$   
196 images or  $\sim 3.2 \times 3.2 \times 10\text{mm}$  for  $^{129}\text{Xe}$  images. To avoid partial volume effects at the  
197 edge of the ventilation-weighted images, the TCV mask was eroded by 1 pixel, and

198 the ventilation-weighted image was then multiplied by the VV mask and eroded TCV  
199 masks, with voxels outside of the VV and TCV masks being excluded from the local  
200 heterogeneity calculation. To generate maps of ventilation heterogeneity, a 3x3 voxel  
201 kernel (~9x9mm) was then passed over the images, centered on every voxel in the  
202 ventilated volume, to calculate the local variation of signal intensity ( $H_{i,j,k}$  at voxel  
203  $i,j,k$ ).  $H_{score}$  in this work was then defined as the median of the non-zero values of the  
204 local heterogeneity map rather than the mean as previously reported, as the  
205 histograms of  $H_{score}$  were not normally distributed. For images acquired at TLC,  
206 where there was clear signal dropout due to coil sensitivity coverage, VV and TCV  
207 masks were matched, i.e. where signal dropout occurred emulating a defect it was  
208 manually excluded on both the TCV and VV masks, in order to ensure that this did  
209 not cause increased  $H_{score}$  and decreased %VV.

210

211 Additionally, the mean  $H_{score}$  of the most posterior slice was compared to the mean  
212  $H_{score}$  of the remaining image slices for each volunteer at each inflation level for the  
213 data acquired with  $^3\text{He}$ . The mean values were grouped by volunteer and lung volume  
214 and significant differences were assessed using either a paired t-test or Wilcoxon  
215 matched-pairs signed rank test depending on the normality of the data. This analysis  
216 was not carried out for  $^{129}\text{Xe}$  data due to the reduced number of subjects.

217

### 218 Repeatability and statistical analysis

219 To assess the repeatability of %VV and  $H_{score}$  between session 1 (S1) and session 2  
220 (S2), the coefficient of variation (CoV), Bland-Altman analysis (2), paired t-tests and  
221 the repeatability limit were used. For CoV analysis, values were grouped by inflation  
222 level and session e.g. RV S1 for all volunteers was compared to RV S2 for all

223 volunteers. Additionally, to assess repeatability in the image domain voxel-wise  
224 correlation (25) was carried out where each of the six same-inflation inter-session  
225 image pairs were spatially aligned via deformable image registration (3), in order to  
226 facilitate computation of Spearman correlation coefficients as previously described  
227 (30). The repeatability limit was calculated as  $1.96 \times \sqrt{2}s_w$ , where  $s_w$  is the within-  
228 subjects standard deviation calculated using SPSS (version 23, IBM) (21).

229

230 Spearman's correlation was also used to assess the relationship between TCV  
231 and %VV and  $H_{score}$  along with the relationship between TCV and the absolute  
232 change of %VV and  $H_{score}$  over the two imaging sessions. Finally, a two-way repeated  
233 measures analysis of variance was performed to statistically validate the effect of lung  
234 volume on  $H_{score}$  and %VV where within subject factors were defined as the imaging  
235 session and lung inflation level, and multiple comparisons were carried out using the  
236 Tukey correction. Voxel-wise correlation and two-way repeated measures analysis of  
237 variance was not carried out for the  $^{129}\text{Xe}$  data due to the reduced number of subjects  
238 scanned.

239

## 240 **Results**

### 241 Comparison of HP $^{129}\text{Xe}$ and HP $^3\text{He}$ MRI at different inflation levels

242 The SNR of the  $^{129}\text{Xe}$  images was lower than the SNR of the  $^3\text{He}$  images, particularly  
243 at RV, RV+1L and FRC, as can be seen in Figure 3. The RV image of HV3 ( $^{129}\text{Xe}$ ,  
244 session 2) had complete loss of signal from posterior sections of the lung due to a coil  
245 sensitivity issue at the time of the experiment and was thus excluded from analysis.  
246  $^{129}\text{Xe}$  images had consistently lower %VV ( $p < 0.0001$ ) and higher  $H_{score}$  ( $p < 0.0001$ )  
247 when compared to those obtained with HP  $^3\text{He}$  (Tables 3 and 4).

248 The effect of lung inflation level on %VV and  $H_{score}$

249 The effect of lung inflation level on  $^3\text{He}$  and  $^{129}\text{Xe}$  images acquired at different lung  
250 volumes is shown in Figure 4 for volunteer 2. There was a trend towards increased  
251 ventilation homogeneity at higher lung volumes, which was seen using both gases.  
252 For  $^3\text{He}$  data significant differences between  $H_{score}$  were found when comparing TLC  
253 to all other lung volumes via the two-way analysis of variance ( $p < 0.0001$  for all). No  
254 other significant differences in  $H_{score}$  between different inflation levels were found.

255

256 %VV also varied with lung volume as can be seen from the mean values of %VV and  
257  $H_{score}$  shown in Table 4 which are visualized in Figure 5. For  $^3\text{He}$  data, %VV at RV  
258 and FRC+1L were the only volumes that were significantly different from each other  
259 when compared using the two-way analysis of variance ( $p = 0.0155$ ). Lung volume had  
260 a significant effect on both %VV ( $p = 0.0265$ ) and  $H_{score}$  ( $p < 0.0001$ ).

261

262 When considering the  $^1\text{H}$  MRI acquired in the same breath as  $^3\text{He}$  MRI, TCV  
263 generated from the  $^1\text{H}$  images correlated strongly with  $H_{score}$  ( $r = -0.75$ ,  $p < 0.0001$ ) but  
264 not with %VV ( $r = 0.27$ ,  $p = 0.15$ ). TCV had a weak correlation with the absolute  
265 change in %VV ( $r = -0.39$ ,  $p = 0.03$ ) but not  $H_{score}$  ( $r = 0.01$ ,  $p = 0.53$ ). For the  $^1\text{H}$  MRI  
266 acquired in a separate breath to the  $^{129}\text{Xe}$  MRI, TCV had a strong correlation with  
267  $H_{score}$  ( $r = -0.90$ ,  $p < 0.0001$ ) and a moderate correlation with the absolute change of  
268  $H_{score}$  over the two sessions ( $r = -0.66$ ,  $p = 0.01$ ). TCV had no significant correlation  
269 with %VV or the absolute change in %VV over both sessions ( $r = 0.44$ ,  $p = 0.12$  and  $r = -$   
270  $0.33$ ,  $p = 0.25$  respectively).

271

272 Regardless of the acquisition volume increased  $H_{\text{score}}$  was seen in the posterior region  
273 of the lung (Figure 6) with the most posterior slice having a mean $\pm$ SD  $H_{\text{score}}$  over all  
274 volunteers and inflation levels of  $15.4\pm 7.1\%$  whilst all other slices combined had  
275 values of  $9.8\pm 3.1\%$  when considering  $^3\text{He}$  data. Additionally, significant differences  
276 between the most posterior slice and the remaining slices (Table 5) of the image were  
277 seen at RV+1L and FRC+1L ( $p=0.0087$  and  $p=0.031$  respectively) whilst no  
278 significant difference was seen at RV, FRC and TLC ( $p = 0.1562$ ,  $p=0.3125$  and  
279  $p=0.0790$  respectively).

280

### 281 Repeatability of %VV and $H_{\text{score}}$

282 Table 6 shows the CoV of %VV and  $H_{\text{score}}$  over all 6 volunteers at each of the lung  
283 volumes imaged with  $^3\text{He}$  and over all 3 volunteers imaged with  $^{129}\text{Xe}$ . For  $^3\text{He}$  data,  
284 CoV was less than 1.5% for %VV and less than 5.5% for  $H_{\text{score}}$  at all lung volumes.  
285 Concerning  $^{129}\text{Xe}$  data, CoV was less than 4% for %VV and less than 10% for  $H_{\text{score}}$   
286 at all lung volumes.

287

288 Concerning the  $^3\text{He}$  data, strong inter-session voxel-wise correlation was observed for  
289 all lung volumes (mean $\pm$ SD Spearman coefficients:  $0.92\pm 0.03$  for RV;  $0.94\pm 0.03$  for  
290 RV+1L;  $0.95\pm 0.02$  for FRC;  $0.95\pm 0.03$  for FRC+1L;  $0.93\pm 0.02$  for TLC).

291

292 Bland-Altman bias $\pm$ limits of agreement (LOA) are visualized in Figures 7 ( $^3\text{He}$ ) and  
293 8 ( $^{129}\text{Xe}$ ) for both %VV (A) and  $H_{\text{score}}$  (B). For  $^3\text{He}$  data, the limits of agreement were  
294 less than 5% for %VV, and less than 2.5% for  $H_{\text{score}}$ . For  $^{129}\text{Xe}$  data, the limits of  
295 agreement were less than 10% for %VV, and less than 4% for  $H_{\text{score}}$ . For  $^3\text{He}$  MRI the  
296 bias for %VV was less than 2% at all lung volumes whilst  $H_{\text{score}}$  bias was less than

297 1% at all lung volumes whilst for  $^{129}\text{Xe}$  MRI %VV bias was less than 6% at all lung  
298 volumes and  $H_{\text{score}}$  bias was less than 2% at all lung volumes.

299

300 Table 7 details the repeatability limit for %VV and  $H_{\text{score}}$  from both HP  $^3\text{He}$  and  $^{129}\text{Xe}$   
301 images. When considering  $^3\text{He}$  data %VV repeatability was less than 3% for all  
302 volumes except RV and less than 2% for all volumes when considering  $H_{\text{score}}$ . When  
303 considering  $^{129}\text{Xe}$  data %VV repeatability was less than 10% for all volumes except  
304 RV and less than 3% for all volumes when considering  $H_{\text{score}}$ .

305

### 306 **Discussion**

307 The work carried out here has demonstrated that lung volume has a significant  
308 bearing on quantitative measurements of lung ventilation derived from both  $^3\text{He}$  and  
309  $^{129}\text{Xe}$  MRI. Additionally, from the effect of lung volume on the quantitative metrics  
310 of %VV and  $H_{\text{score}}$  evident in healthy volunteers, it can be concluded that the lung  
311 volume during imaging must be well controlled to ensure that these metrics can be  
312 used reliably in longitudinal studies.

313

314 Imaging over all volunteers revealed increased ventilation heterogeneity at lower lung  
315 volumes, potentially indicating partial airway closure in certain regions of the lung.  
316 Increased heterogeneity was particularly observed in the posterior section of the lung  
317 at RV+1L, exemplified by the median  $H_{\text{score}}$  per slice plotted against slice number for  
318 V5 in Figure 9. This increased heterogeneity is likely due to the breathing maneuver  
319 used to obtain the images at RV+1L, that is the volunteers first exhaled to RV, which  
320 may have caused some airway closure. In contrast, the HP gas mixture was inhaled  
321 from FRC for all other lung volumes, and so the ventilation seen in the RV and FRC

322 images was influenced by the gas distribution within the lungs at FRC+1L. Note that  
323 although increased heterogeneity is seen in the anterior portion of the lung, the  
324 increased  $H_{\text{score}}$  in those areas are due to the reduced SNR due to decreased gas  
325 reaching those areas within the lung.

326

327 This increased ventilation heterogeneity at RV+1L in volunteers suggests the same  
328 underpinning mechanisms as reported in the work by Muradyan et al. (23), where  
329 there were distinct focal areas of lung affected by airway closure after inhalation of  
330 small gas volumes from below residual volume in elite divers. We hypothesize that  
331 the areas of decreased ventilation signal at RV+1L were caused by airways remaining  
332 closed following inhalation of the gas mixture. We believe that this same effect was  
333 not observed at RV in the current study since the maneuver to RV required first  
334 inhaling to FRC+1L, such that gas would remain in the areas opened by this first  
335 inhalation maneuver even if the airways were to close later on. The areas of reduced  
336 ventilation in lungs of the elite divers following inhalation from sub-RV levels  
337 observed in the work by Muradyan et al. (23) were larger than those seen here in these  
338 volunteers, whilst they did not see the same heterogeneity seen here in their  
339 volunteers following inhalation from RV. One possible reason for this is the  
340 improvements in the image resolution for  $^{129}\text{Xe}$  when compared to their experiments  
341 that were carried out with 2D projection imaging, and thus providing us with better  
342 spatial sampling of regional heterogeneity.

343

344 Imaging after smaller inspirations from RV would be interesting in order to assess at  
345 which point the ventilation heterogeneity would return to a distribution closer to that  
346 seen at FRC or FRC+1L. In this case, it would be expected that the smaller the



347 volume inhaled from RV, the greater the ventilation heterogeneity would be; although  
348 the feasibility of these experiments would be limited by the volume of HP gas  
349 required for sufficient image SNR if carrying the experiment out with  $^{129}\text{Xe}$ . Another  
350 factor which may contribute to increased  $H_{\text{score}}$  at RV when compared to FRC+1L and  
351 FRC is the increased ratio of blood vessel volume to lung volume at RV, resulting in  
352 increased  $H_{\text{score}}$ .

353

354 The small CoV of %VV between sessions further confirms the growing body of  
355 evidence that %VV is a robust global metric of lung ventilation (5, 12, 17), and the  
356 high inter-scan repeatability makes %VV (or VDP) a good candidate metric for  
357 longitudinal assessment of lung function in patients (17). The proportionally larger  
358 CoV of the  $H_{\text{score}}$  suggests that this measure of global ventilation image heterogeneity  
359 may be less repeatable.

360

361 The generally lower SNR of  $^{129}\text{Xe}$  images when compared to  $^3\text{He}$  images is a well-  
362 known phenomenon and follows previous publications (14, 28), with  $^{129}\text{Xe}$   
363 acquisitions having a mean $\pm$ SD SNR of  $30\pm 13$  compared to the  $42\pm 15$  of the  $^3\text{He}$   
364 acquisitions. Consequently, the higher  $H_{\text{score}}$  seen in the  $^{129}\text{Xe}$  images when compared  
365 to images acquired with HP  $^3\text{He}$  is at least partially due to the lower SNR and thus  
366 increased heterogeneity of signal within ventilated regions. The lower %VV values  
367 measured from  $^{129}\text{Xe}$  images compared to  $^3\text{He}$  images may be due to the lower  
368 diffusivity of  $^{129}\text{Xe}$  compared to  $^3\text{He}$ , and are consistent with %VV values reported  
369 previously in healthy volunteers, patients with chronic obstructive pulmonary disease  
370 and patients with lung cancer who were imaged with both gases (18, 27). Furthermore,  
371 lower SNR in one of the  $^{129}\text{Xe}$  acquisitions (V6, RV, S1) caused an increase in  $H_{\text{score}}$

372 showing that the maneuvers or gas doses need to be optimized for the  $^{129}\text{Xe}$  imaging  
373 acquisitions if this methodology is applied to patient cohorts. The need to register the  
374 anatomical images to the ventilation images for  $^{129}\text{Xe}$  %VV calculation will also  
375 contribute to the lower repeatability of  $^{129}\text{Xe}$  %VV when compared to  $^3\text{He}$  %VV (12),  
376 where anatomical images were acquired in the same breath-hold. Additionally, due to  
377 imaging constraints, HP  $^{129}\text{Xe}$  images were acquired with double the slice thickness  
378 (10mm) of the HP  $^3\text{He}$  images (5mm); thus, differences would be expected due to  
379 different inherent physical properties and image acquisition considerations of the  
380 respective gas.

381

382 Imaging patients with HP gas at different lung volumes may provide a clearer picture  
383 of the nature of lung disease. For example, in patients with obstructive lung disease,  
384 following deep inhalation to TLC, the effect of increased positive pressure within the  
385 airways may result in a reduced  $H_{\text{score}}$  and increased %VV due to opening of  
386 obstructed airways (20). Additionally, as patients with chronic respiratory disease  
387 may have increased closing volumes, imaging at expiration may identify areas of gas  
388 trapping similar to those observed by Holmes et al. (9-11).

389

390 An increased number of healthy volunteers with a larger age range, and inclusion of  
391 female subjects would extend this preliminary work into the effect of lung volume on  
392 ventilation heterogeneity in healthy volunteers. Additionally, mitigating the signal  
393 dropout seen in TLC images with larger coil coverage is an important consideration  
394 for future studies. The smoking history of four of the six volunteers (two former  
395 smokers and two occasional smokers) means that these data may not represent the  
396 ventilation patterns seen in a group of healthy never-smokers. However, the number

397 of pack years reported by the volunteers scanned was low ( $<0.7$ ), and in a previous  
398  $^3\text{He}$  MRI study of pulmonary ventilation (26) three of the smokers would have been  
399 classified as never-smokers ( $<0.5$  pack years). However, the volunteers scanned were  
400 spirometrically defined as free from respiratory disease and not unrepresentative of  
401 the general population in terms of smoking history. The fact that increased ventilation  
402 heterogeneity at lower lung inflation levels was seen in the two never smokers as well  
403 as those with a smoking history suggests this effect is not due to smoking related  
404 obstructive airways disease.

405

#### 406 **Conclusions**

407 Increased ventilation heterogeneity was observed in HP gas images acquired at lower  
408 lung volumes in healthy volunteers. This work has shown that although TLV and VV  
409 may vary considerably between repeated scans there was little effect on %VV in these  
410 healthy volunteers. This indicates it may be important to image patients over a range  
411 of lung volumes with different breathing maneuvers to fully understand disease  
412 progression and accurately characterize ventilation defects and pulmonary mechanics.  
413 Finally, the variation in lung volume must be considered when monitoring patients  
414 longitudinally with hyperpolarized gas MRI particularly in the cases of disease with a  
415 reversible nature such as asthma.

416

417 **Acknowledgements:** The authors thank Mr. Oliver Rodgers for aiding with the  
418 scanning of volunteers.

419

420 **Grants:** The authors thank the University of Sheffield, the HEE/NIHR (NIHR-RP-  
421 R3-12-027, ICA-CDRF-2015-01-027), Sheffield Hospitals Charity (161731) and the  
422 MRC (MR/M008894/1) for funding this research.

423

424 **Disclosures:** Paul J.C. Hughes – PhD part-funded by GlaxoSmithKline  
425 (STU100037614).

426

427 **References**

- 428 1. **Altes TA, Meyer CH, Mata JF, Froh DK, Paget-Brown A, Teague WG,**  
429 **Fain SB, de Lange EE, Ruppert K, and Botfield MC.** Hyperpolarized helium-3  
430 magnetic resonance lung imaging of non-sedated infants and young children: a proof-  
431 of-concept study. *Clinical imaging* 45: 105-110, 2017.
- 432 2. **Altman DG, and Bland JM.** Measurement in medicine: the analysis of  
433 method comparison studies. *The statistician* 307-317, 1983.
- 434 3. **Avants BB, Tustison NJ, Song G, Cook PA, Klein A, and Gee JC.** A  
435 reproducible evaluation of ANTs similarity metric performance in brain image  
436 registration. *NeuroImage* 54: 2033-2044, 2011.
- 437 4. **Bannier E, Cieslar K, Mosbah K, Aubert F, Duboeuf F, Salhi Z, Gaillard**  
438 **S, Berthezène Y, Crémillieux Y, and Reix P.** Hyperpolarized 3He MR for sensitive  
439 imaging of ventilation function and treatment efficiency in young cystic fibrosis  
440 patients with normal lung function. *Radiology* 255: 225-232, 2010.
- 441 5. **Fain SB, Korosec FR, Holmes JH, O'Halloran R, Sorkness RL, and Grist**  
442 **TM.** Functional lung imaging using hyperpolarized gas MRI. *Journal of Magnetic*  
443 *Resonance Imaging* 25: 910-923, 2007.
- 444 6. **Guo F, Yuan J, Rajchl M, Svenningsen S, Capaldi DP, Sheikh K, Fenster**  
445 **A, and Parraga G.** Globally optimal co-segmentation of three-dimensional  
446 pulmonary 1 H and hyperpolarized 3 He MRI with spatial consistence prior. *Medical*  
447 *image analysis* 23: 43-55, 2015.
- 448 7. **He M, Driehuys B, Que LG, and Huang Y-CT.** Using hyperpolarized  
449 129Xe MRI to quantify the pulmonary ventilation distribution. *Academic radiology*  
450 23: 1521-1531, 2016.
- 451 8. **Heydarian M, Kirby M, Wheatley A, Fenster A, and Parraga G.** Two and  
452 three-dimensional segmentation of hyperpolarized 3 He magnetic resonance imaging  
453 of pulmonary gas distribution. In: *Medical Imaging 2012: Biomedical Applications in*  
454 *Molecular, Structural, and Functional Imaging* International Society for Optics and  
455 Photonics, 2012, p. 83171C.
- 456 9. **Holmes JH, Korosec FR, Du J, O'halloran RL, Sorkness RL, Grist TM,**  
457 **Kuhlman JE, and Fain SB.** Imaging of lung ventilation and respiratory dynamics in  
458 a single ventilation cycle using hyperpolarized He- 3 MRI. *Journal of Magnetic*  
459 *Resonance Imaging* 26: 630-636, 2007.
- 460 10. **Holmes JH, O'halloran RL, Brodsky EK, Bley TA, Francois CJ, Velikina**  
461 **JV, Sorkness RL, Busse WW, and Fain SB.** Three- dimensional imaging of  
462 ventilation dynamics in asthmatics using multiecho projection acquisition with  
463 constrained reconstruction. *Magnetic resonance in medicine* 62: 1543-1556, 2009.
- 464 11. **Holmes JH, O'Halloran RL, Brodsky EK, Jung Y, Block WF, and Fain**  
465 **SB.** 3D hyperpolarized He- 3 MRI of ventilation using a multi- echo projection  
466 acquisition. *Magnetic resonance in medicine* 59: 1062-1071, 2008.
- 467 12. **Horn F, Tahir B, Stewart N, Collier G, Norquay G, Leung G, Ireland R,**  
468 **Parra- Robles J, Marshall H, and Wild J.** Lung ventilation volumetry with same-  
469 breath acquisition of hyperpolarized gas and proton MRI. *NMR in biomedicine* 27:  
470 1461-1467, 2014.
- 471 13. **Horn FC, Marshall H, Collier GJ, Kay R, Siddiqui S, Brightling CE,**  
472 **Parra-Robles J, and Wild JM.** Regional Ventilation Changes in the Lung:  
473 Treatment Response Mapping by Using Hyperpolarized Gas MR Imaging as a  
474 Quantitative Biomarker. *Radiology* 284: 854-861, 2017.

- 475 14. **Horn FC, Rao M, Stewart NJ, and Wild JM.** Multiple breath washout of  
476 hyperpolarized  $^{129}\text{Xe}$  and  $^3\text{He}$  in human lungs with three- dimensional balanced  
477 steady- state free- precession imaging. *Magnetic resonance in medicine* 77: 2288-  
478 2295, 2017.
- 479 15. **Hughes PJ, Horn FC, Collier GJ, Biancardi A, Marshall H, and Wild JM.**  
480 Spatial fuzzy c- means thresholding for semiautomated calculation of percentage lung  
481 ventilated volume from hyperpolarized gas and  $^1\text{H}$  MRI. *Journal of Magnetic*  
482 *Resonance Imaging* 47: 640-646, 2018.
- 483 16. **Kirby M, Heydarian M, Svenningsen S, Wheatley A, McCormack DG,**  
484 **Etemad-Rezai R, and Parraga G.** Hyperpolarized  $^3\text{He}$  Magnetic Resonance  
485 Functional Imaging Semiautomated Segmentation. *Academic radiology* 19: 141-152,  
486 2012.
- 487 17. **Kirby M, Mathew L, Wheatley A, Santyr GE, McCormack DG, and**  
488 **Parraga G.** Chronic obstructive pulmonary disease: longitudinal hyperpolarized  $^3\text{He}$   
489 MR imaging. *Radiology* 256: 280-289, 2010.
- 490 18. **Kirby M, Svenningsen S, Owrangi A, Wheatley A, Farag A, Ouriadov A,**  
491 **Santyr GE, Etemad-Rezai R, Coxson HO, and McCormack DG.** Hyperpolarized  
492  $^3\text{He}$  and  $^{129}\text{Xe}$  MR imaging in healthy volunteers and patients with chronic  
493 obstructive pulmonary disease. *Radiology* 265: 600-610, 2012.
- 494 19. **Marshall H, Horsley A, Taylor CJ, Smith L, Hughes D, Horn FC, Swift**  
495 **AJ, Parra-Robles J, Hughes PJ, and Norquay G.** Detection of early subclinical  
496 lung disease in children with cystic fibrosis by lung ventilation imaging with  
497 hyperpolarised gas MRI. *Thorax* 72: 760-762, 2017.
- 498 20. **Marshall H, Siddiqui S, Leung G, Parra-Robles J, Xu X, Brightling C,**  
499 **and Wild J.** Imaging The Effect Of Airway Opening In Asthma Due To Inflation  
500 State With  $^3\text{He}$  MRI. In: *B109 TECHNOLOGIC ADVANCES IN IMAGING FOR*  
501 *PHENOTYPING LUNG DISEASE* Am Thoracic Soc, 2013, p. A3744-A3744.
- 502 21. **McAlinden C, Khadka J, and Pesudovs K.** Precision (repeatability and  
503 reproducibility) studies and sample-size calculation. *Journal of Cataract & Refractive*  
504 *Surgery* 41: 2598-2604, 2015.
- 505 22. **Miller MR, Hankinson J, Brusasco V, Burgos F, Casaburi R, Coates A,**  
506 **Crapo R, Enright Pv, Van Der Grinten C, and Gustafsson P.** Standardisation of  
507 spirometry. *European respiratory journal* 26: 319-338, 2005.
- 508 23. **Muradyan I, Loring SH, Ferrigno M, Lindholm P, Topulos GP, Patz S,**  
509 **and Butler JP.** Inhalation heterogeneity from subresidual volumes in elite divers.  
510 *Journal of Applied Physiology* 109: 1969-1973, 2010.
- 511 24. **Norquay G, Parnell SR, Xu X, Parra-Robles J, and Wild JM.** Optimized  
512 production of hyperpolarized  $^{129}\text{Xe}$  at 2 bars for in vivo lung magnetic resonance  
513 imaging. *Journal of Applied Physics* 113: 044908, 2013.
- 514 25. **Reinstein DZ, Archer TJ, Silverman RH, and Coleman DJ.** Accuracy,  
515 repeatability, and reproducibility of Artemis very high-frequency digital ultrasound  
516 arc-scan lateral dimension measurements. *Journal of Cataract & Refractive Surgery*  
517 32: 1799-1802, 2006.
- 518 26. **Sheikh K, Paulin GA, Svenningsen S, Kirby M, Paterson NA,**  
519 **McCormack DG, and Parraga G.** Pulmonary ventilation defects in older never-  
520 smokers. *Journal of applied physiology* 117: 297-306, 2014.
- 521 27. **Stewart N, Chan H-F, Hughes PJC, Horn FC, Norquay G, Rao M, Yates**  
522 **DP, Ireland RH, Hatton MQ, Tahir BA, Ford P, Swift AJ, Lawson R, Marshall**  
523 **H, Collier GJ, and Wild JM.** Comparison of  $^3\text{He}$  and  $^{129}\text{Xe}$  MRI for evaluation of

- 524 lung microstructure and ventilation at 1.5 T. *Journal of Magnetic Resonance Imaging*,  
525 2018.
- 526 28. **Stewart NJ, Norquay G, Griffiths PD, and Wild JM.** Feasibility of human  
527 lung ventilation imaging using highly polarized naturally abundant xenon and  
528 optimized three- dimensional steady- state free precession. *Magnetic resonance in*  
529 *medicine* 74: 346-352, 2015.
- 530 29. **Svenningsen S, Kirby M, Starr D, Leary D, Wheatley A, Maksym GN,**  
531 **McCormack DG, and Parraga G.** Hyperpolarized <sup>3</sup>He and <sup>129</sup>Xe MRI: differences  
532 in asthma before bronchodilation. *Journal of Magnetic Resonance Imaging* 38: 1521-  
533 1530, 2013.
- 534 30. **Tahir B, Hughes P, Robinson S, Marshall H, Stewart N, Norquay G,**  
535 **Biancardi A, Chan H-F, Collier G, and Hart K.** Spatial comparison of CT-based  
536 surrogates of lung ventilation with hyperpolarized Helium-3 and Xenon-129 gas MRI  
537 in patients undergoing radiation therapy. *International Journal of Radiation*  
538 *Oncology• Biology• Physics* 2018.
- 539 31. **Tzeng Y-S, Lutchen K, and Albert M.** The difference in ventilation  
540 heterogeneity between asthmatic and healthy subjects quantified using hyperpolarized  
541 <sup>3</sup>He MRI. *Journal of Applied Physiology* 106: 813-822, 2009.
- 542 32. **Wanger J, Clausen J, Coates A, Pedersen O, Brusasco V, Burgos F,**  
543 **Casaburi R, Crapo R, Enright P, and Van Der Grinten C.** Standardisation of the  
544 measurement of lung volumes. *European Respiratory Journal* 26: 511-522, 2005.
- 545 33. **Woodhouse N, Wild JM, Paley MN, FICHELE S, Said Z, Swift AJ, and van**  
546 **Beek EJ.** Combined helium- <sup>3</sup>/proton magnetic resonance imaging measurement of  
547 ventilated lung volumes in smokers compared to never- smokers. *Journal of magnetic*  
548 *resonance imaging* 21: 365-369, 2005.
- 549 34. **Zha W, Niles DJ, Kruger SJ, Dardzinski BJ, Cadman RV, Mummy DG,**  
550 **Nagle SK, and Fain SB.** Semiautomated ventilation defect quantification in exercise-  
551 induced bronchoconstriction using hyperpolarized helium-3 magnetic resonance  
552 imaging: a repeatability study. *Academic radiology* 23: 1104-1114, 2016.
- 553

554

555 **FIGURE LEGENDS**

556 **Figure 1** Example of local  $H_{\text{score}}$  calculation in the RV+1L ventilation-weighted  
557 image of volunteer 5 (top image). The yellow box on the left shows an area of low  
558  $H_{\text{score}}$  (enhanced image on the left, with the local area outlined and the voxel that is  
559 replaced denoted with an 'x'), which is highlighted with the blue box in the  $H_{\text{score}}$  map  
560 (lower image). The same is shown for a region of high  $H_{\text{score}}$  on the right.

561 **Figure 2** Breathing maneuvers and acquisition volumes used in this study. Solid gray  
562 lines indicate an inhalation from a 1L bag, solid black lines indicate an exhalation and  
563 dashed gray lines indicate an inhalation of room air. Solid boxes represent acquisition  
564 volumes and dashed boxes represent intermediate volumes as part of the breathing  
565 maneuver.

566 **Figure 3** Signal-to-noise ratio (SNR) values from the volunteers scanned with both  
567  $^3\text{He}$  and  $^{129}\text{Xe}$  only.

568 **Figure 4** Representative slices from all acquisition volumes in V2 from both  $^3\text{He}$  and  
569  $^{129}\text{Xe}$  images. The top row shows the  $^3\text{He}$  images and the bottom row the  $^{129}\text{Xe}$   
570 images acquired in V2.

571 **Figure 5** Plots of (A) percentage lung ventilated volume from  $^3\text{He}$  data, (B)  $H_{\text{score}}$  (%)  
572 from  $^3\text{He}$  data, (C) percentage lung ventilated volume from  $^{129}\text{Xe}$  data and (D)  $H_{\text{score}}$   
573 (%) from  $^{129}\text{Xe}$  data at each acquisition volume. Each circle represents a volunteer  
574 whilst the lines represent the mean of the values.

575 **Figure 6** Representative posterior slices of HP  $^3\text{He}$  ventilation images and  
576 heterogeneity maps at all acquisition volumes from V2. The arrows are pointing to  
577 areas of decreased ventilation and increased  $H_{\text{score}}$ .



578 **Figure 7** Bland-Altman plots of (A) %VV and (B)  $H_{\text{score}}$  generated from images  
579 acquired with HP  $^3\text{He}$  at all acquisition volumes. Black dots indicate bias, gray dots  
580 are the 95% confidence intervals and the black dashed line is 0.

581 **Figure 8** Bland-Altman plots of (A) %VV and (B)  $H_{\text{score}}$  generated from images  
582 acquired with HP  $^{129}\text{Xe}$  at all acquisition volumes. Black dots indicate bias, gray dots  
583 are the 95% confidence intervals and the black dashed line is 0.

584 **Figure 9** Exemplary plot of  $H_{\text{score}}$  from anterior to posterior for V5.

585

*Table 1 Subject demographics. V = volunteer, FEV<sub>1</sub> = Forced expiratory volume in 1 second % predicted*

<b>Subject</b>	<b>Age, yr</b>	<b>Height, cm</b>	<b>Weight, kg</b>	<b>FEV<sub>1</sub></b>	<b>Pack years</b>
<b>V1</b>	32	183.0	87.0	102.0	0.15
<b>V2</b>	35	184.0	76.0	77.2	0.13
<b>V3</b>	31	182.0	83.0	105.0	0.06
<b>V4</b>	34	185.6	94.0	83.6	0.70
<b>V5</b>	27	189.5	74.0	102.9	0
<b>V6</b>	28	187.6	90.0	99.9	0

*Table 2 Gas doses for hyperpolarized (HP) helium-3 ( $^3\text{He}$ ) and xenon-129 ( $^{129}\text{Xe}$ ) acquisitions reported as HP gas dose ( $N_2$ ), where  $N_2$  = nitrogen.  $RV$  = residual volume,  $RV+1L$  = residual volume plus 1 liter of gas mixture,  $FRC$  = functional residual capacity,  $FRC+1L$  = functional residual capacity volume plus 1 liter of gas mixture and  $TLC$  = total lung capacity*

<b>Acquisition</b>	<b><math>^3\text{He}</math> (<math>N_2</math>), ml</b>	<b><math>^{129}\text{Xe}</math> (<math>N_2</math>), ml</b>
<b>RV</b>	200 (800)	1000 (0)
<b>RV+1L</b>	150 (850)	750 (250)
<b>FRC</b>	200 (800)	1000 (0)
<b>FRC+1L</b>	150 (850)	600 (400)
<b>TLC</b>	200 (800)	750 (250)

*Table 3 Mean percentage lung ventilated volume (%VV) and median score of the heterogeneity map ( $H_{score}$ ) values at each lung volume and session (session 1 (S1)/session 2 (S2)) over all volunteers derived from hyperpolarized helium-3 ( $^3\text{He}$ ) and xenon-129 ( $^{129}\text{Xe}$ )*

	<b>RV S1</b>	<b>RV S2</b>	<b>RV+1L S1</b>	<b>RV+1L S2</b>	<b>FRC S1</b>	<b>FRC S2</b>	<b>FRC+1L S1</b>	<b>FRC+1L S2</b>	<b>TLC S1</b>	<b>TLC S2</b>
<b>%VV <math>^3\text{He}</math></b>	95.65	97.17	97.39	97.84	97.30	97.80	98.18	98.05	97.33	97.98
<b><math>H_{score}</math> <math>^3\text{He}</math></b>	10.47	9.98	10.12	10.1	9.37	9.23	9.10	9.20	7.55	7.39
<b>%VV <math>^{129}\text{Xe}</math></b>	82.94	87.43	92.36	90.86	93.53	94.99	92.99	96.55	95.83	94.98
<b><math>H_{score}</math> <math>^{129}\text{Xe}</math></b>	15.89	14.92	11.51	12.29	10.83	10.99	11.09	10.53	8.71	8.24

Table 4 Average percentage lung ventilated volume (%VV) and median score of the heterogeneity map ( $H_{score}$ ) values over session 1 and session 2 generated from hyperpolarized helium-3 ( $^3\text{He}$ ) and xenon-129 ( $^{129}\text{Xe}$ ) images for the three volunteers (V) scanned with both gases

Acquisition	%VV $^3\text{He}$ V2	%VV $^{129}\text{Xe}$ V2	%VV $^3\text{He}$ V3	%VV $^{129}\text{Xe}$ V3	%VV $^3\text{He}$ V6	%VV $^{129}\text{Xe}$ V6
<b>RV</b>	98.68	96.26	97.03	NA	95.41	88.88
<b>RV+1L</b>	97.67	90.46	99.49	91.54	98.26	92.84
<b>FRC</b>	98.85	97.53	98.34	94.41	97.85	90.85
<b>FRC+1L</b>	98.46	96.70	98.76	94.51	98.10	93.11
<b>TLC</b>	99.46	95.58	99.12	93.14	97.82	97.50
Acquisition	$H_{score}$ $^3\text{He}$ V2	$H_{score}$ $^{129}\text{Xe}$ V2	$H_{score}$ $^3\text{He}$ V3	$H_{score}$ $^{129}\text{Xe}$ V3	$H_{score}$ $^3\text{He}$ V6	$H_{score}$ $^{129}\text{Xe}$ V6
<b>RV</b>	8.96	12.53	11.63	NA	10.16	16.16
<b>RV+1L</b>	10.26	12.08	8.82	11.74	9.04	11.89
<b>FRC</b>	8.85	11.01	9.15	10.91	8.90	10.82
<b>FRC+1L</b>	9.33	10.83	8.61	10.62	8.59	10.98
<b>TLC</b>	6.15	8.10	7.33	8.95	6.50	8.38

Table 5 Mean  $H_{score}$  (over session 1 and session 2) at the most posterior slice and all remaining slices for all volunteers at each lung volume for all images acquired using hyperpolarized helium-3

Volunteer	RV		RV+1L		FRC		FRC+1L		TLC	
	Posterior slice	Remaining slices	Posterior slice	Remaining slices	Posterior slice	Remaining slices	Posterior slice	Remaining slices	Posterior slice	Remaining slices
<b>V1</b>	14.95	11.75	21.38	12.11	23.9	12.19	21.13	10.72	17.45	10.3
<b>V2</b>	12.68	9.13	23.97	11.62	15.11	9.30	23.59	10.22	9.28	6.85
<b>V3</b>	8.28	11.15	18.18	8.58	5.59	9.06	10.16	8.65	7.64	7.40
<b>V4</b>	20.23	10.91	17.83	10.24	18.15	10.65	20.46	10.74	25.71	9.39
<b>V5</b>	9.98	10.98	27.03	11.03	5.37	9.42	9.53	9.60	8.29	8.25
<b>V6</b>	15.57	11.00	9.58	9.57	11.53	9.40	13.60	9.02	27.03	7.18

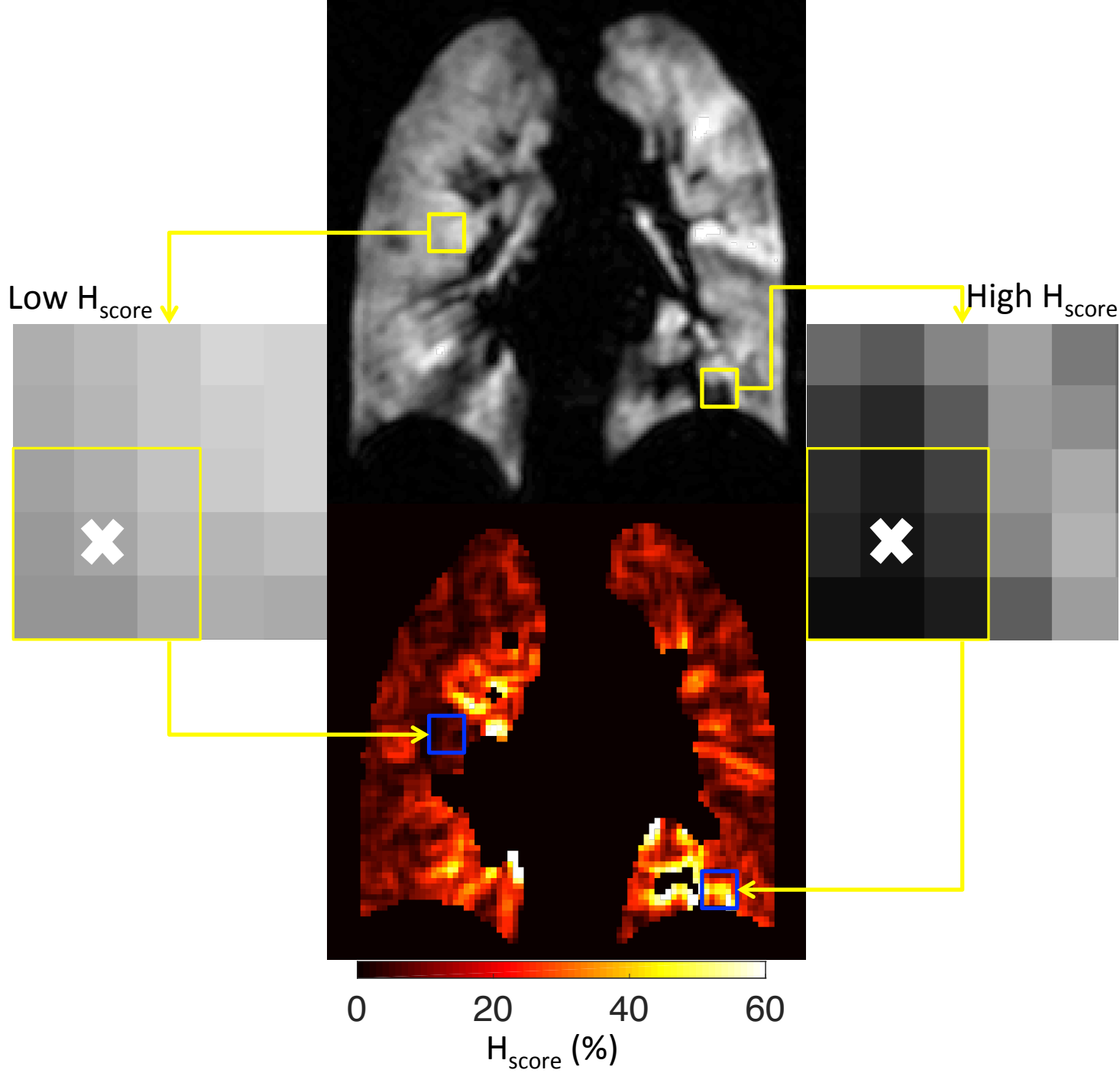
Table 6 Coefficient of variation (CoV) at each inflation level for metrics derived from hyperpolarized helium-3 ( $^3\text{He}$ ) and xenon-129 ( $^{129}\text{Xe}$ )

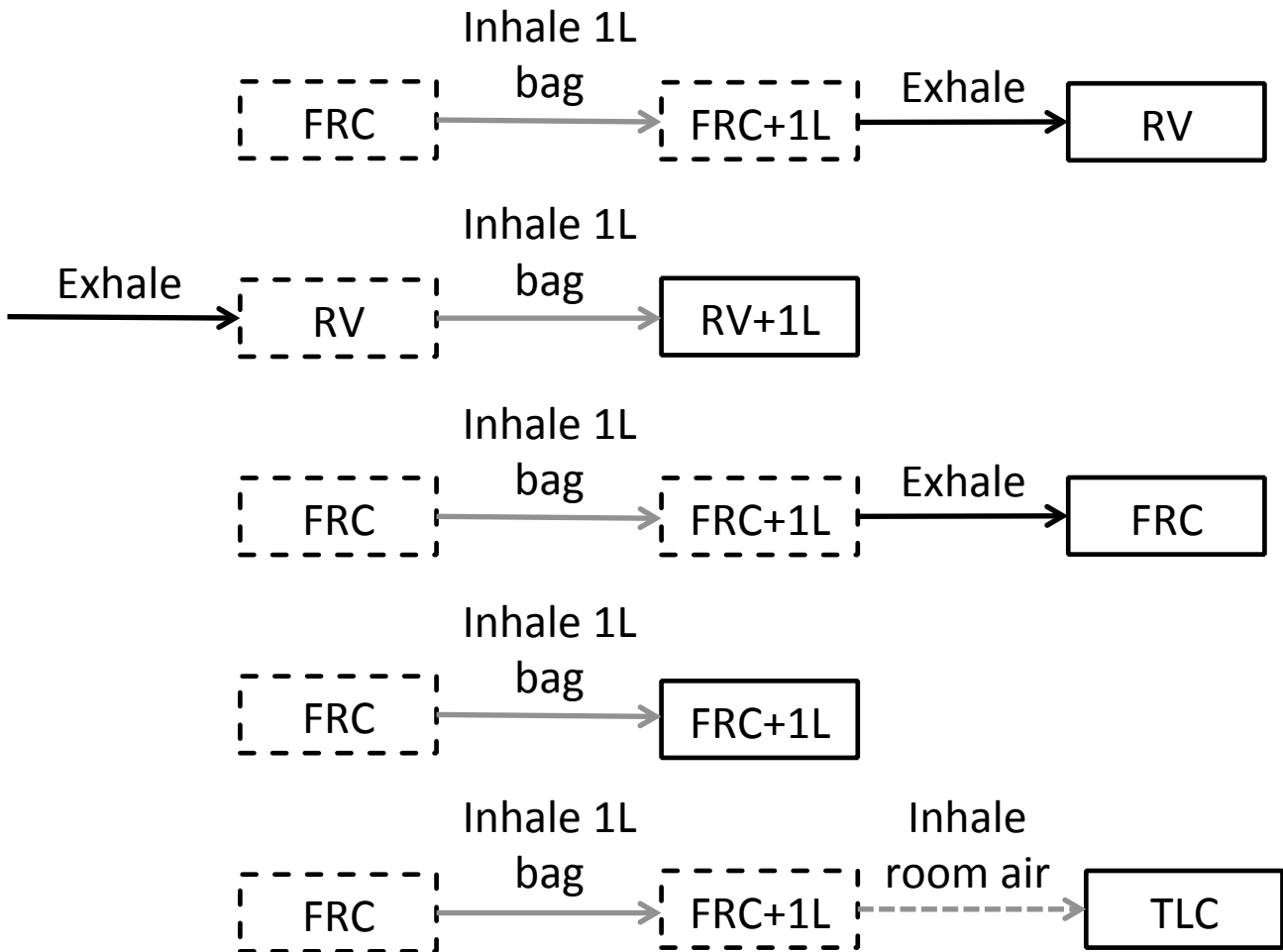
$^3\text{He}$					$^{129}\text{Xe}$				
Acquisition	TLV	VV	%VV	H <sub>score</sub>	Acquisition	TLV	VV	%VV	H <sub>score</sub>
<b>RV</b>	3.40	3.05	1.29	5.32	<b>RV</b>	3.33	1.34	3.98	9.37
<b>RV+1L</b>	4.13	4.64	0.63	4.62	<b>RV+1L</b>	2.19	2.26	1.16	7.60
<b>FRC</b>	4.63	4.64	0.87	3.99	<b>FRC</b>	5.88	4.80	1.49	2.86
<b>FRC+1L</b>	3.42	3.42	0.38	2.74	<b>FRC+1L</b>	6.88	6.00	3.18	3.74
<b>TLC</b>	1.19	1.00	0.54	5.46	<b>TLC</b>	1.97	1.91	0.62	4.62

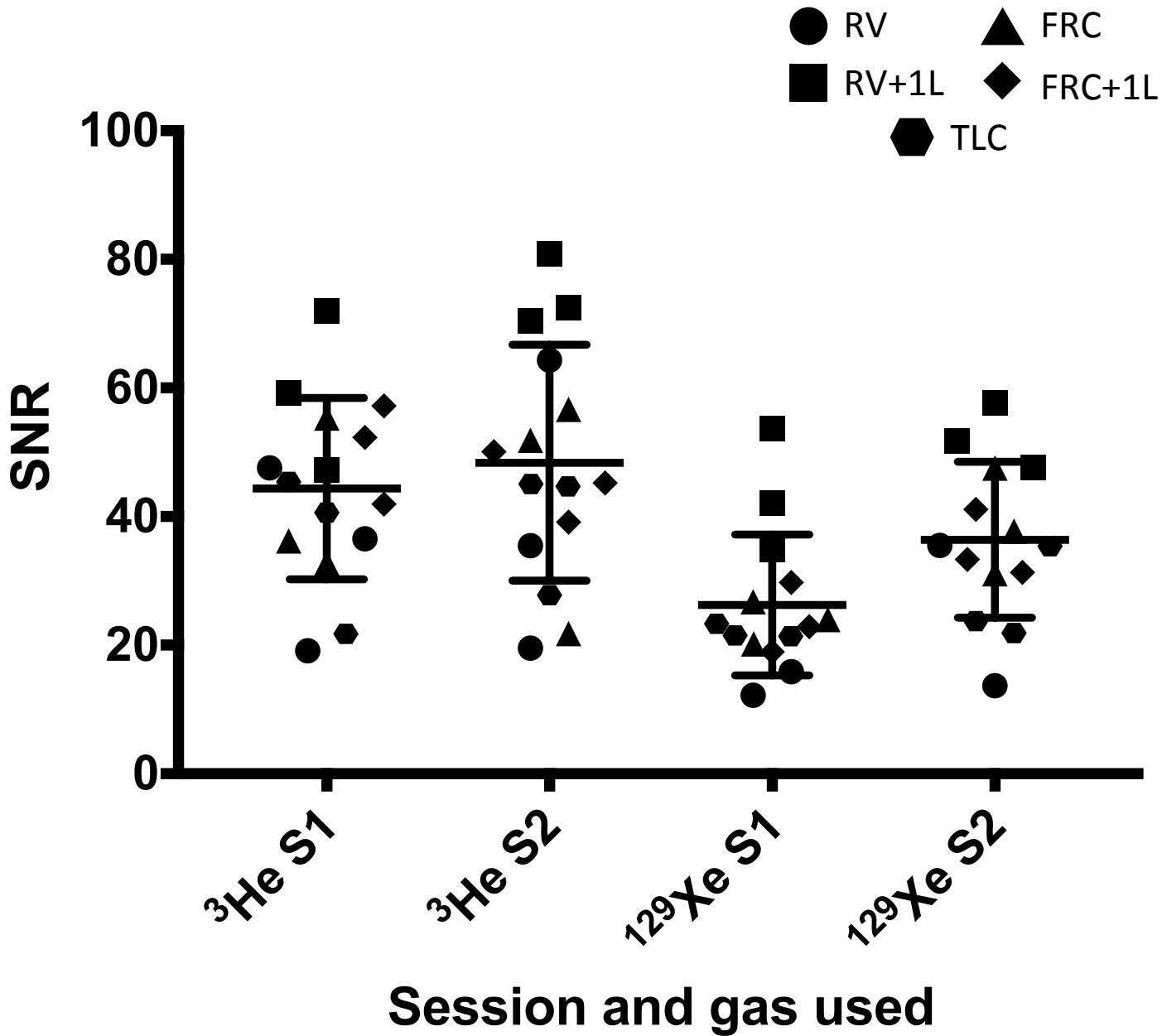
Table 7 Repeatability limit for percentage lung ventilated volume (%VV) and median value of the heterogeneity map ( $H_{score}$ ) for images acquired using hyperpolarized helium-3 ( $^3\text{He}$ ) and xenon-129 ( $^{129}\text{Xe}$ )

Acquisition	$^3\text{He}$ %VV	$^3\text{He}$ $H_{score}$	$^{129}\text{Xe}$ %VV	$^{129}\text{Xe}$ $H_{score}$
<b>RV</b>	5.08	1.80	11.69	3.72
<b>RV+1L</b>	2.19	1.86	3.06	2.62
<b>FRC</b>	2.90	1.29	4.50	1.07
<b>FRC+1L</b>	1.39	0.80	9.59	1.45
<b>TLC</b>	2.02	1.35	1.95	1.36

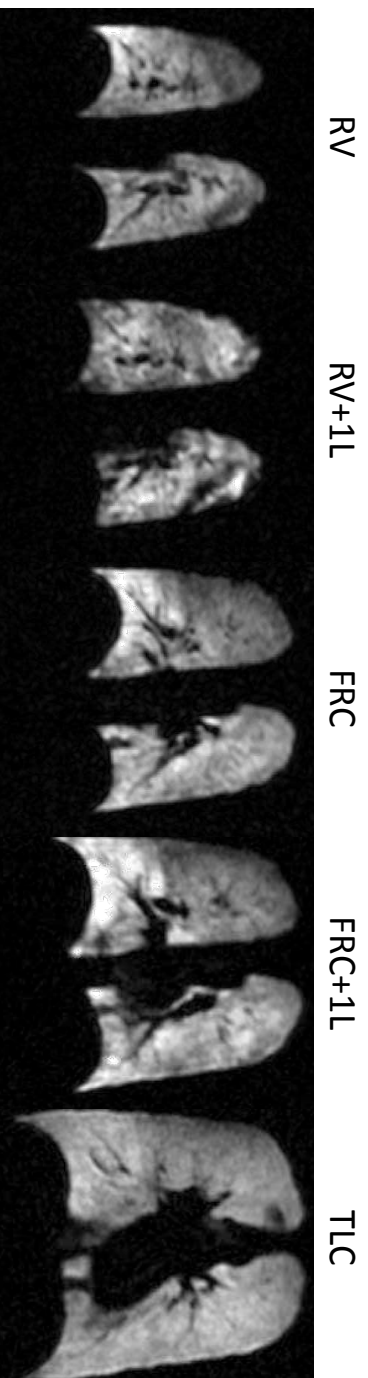




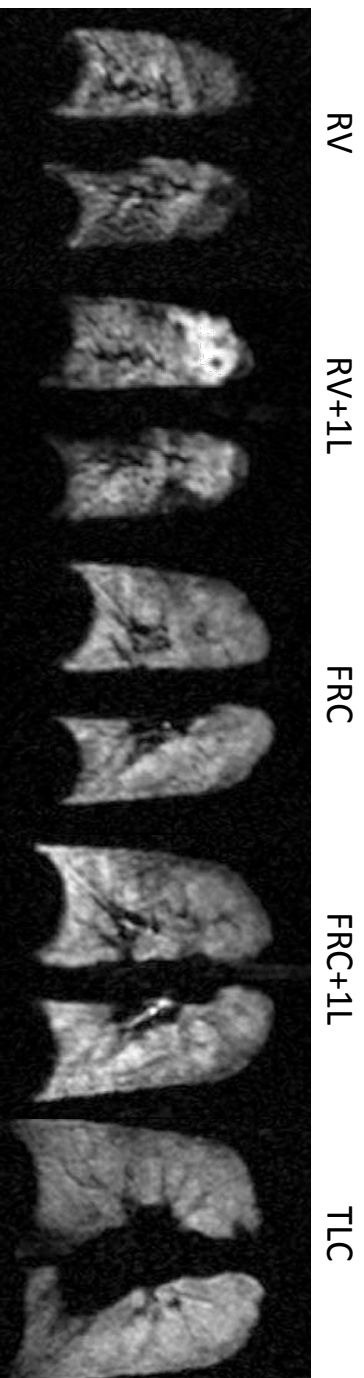


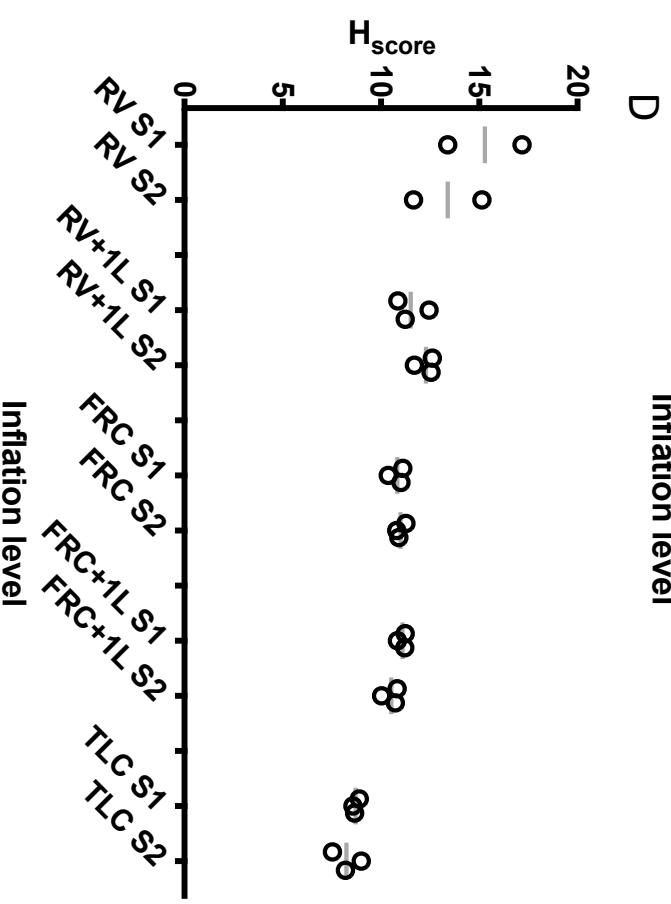
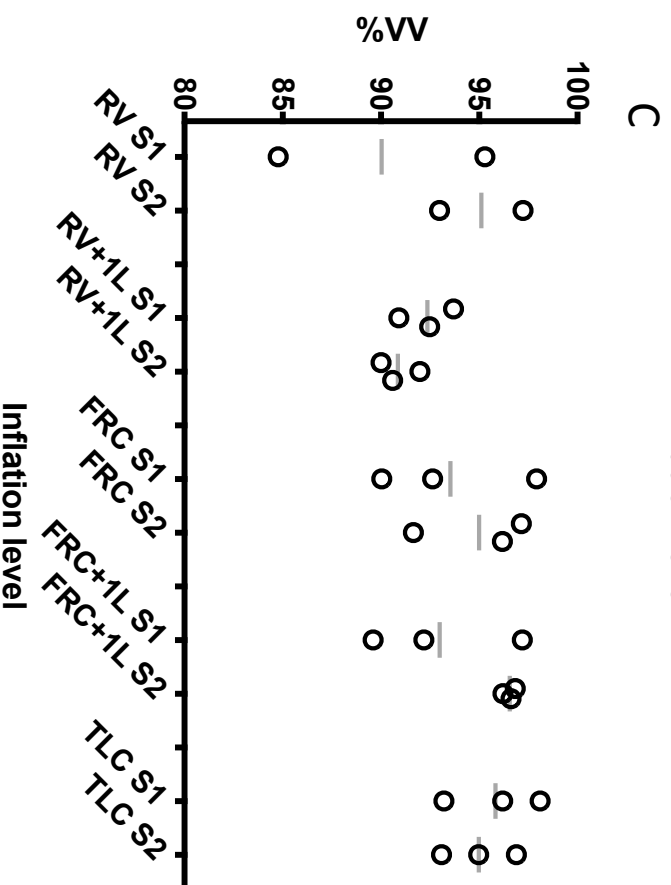
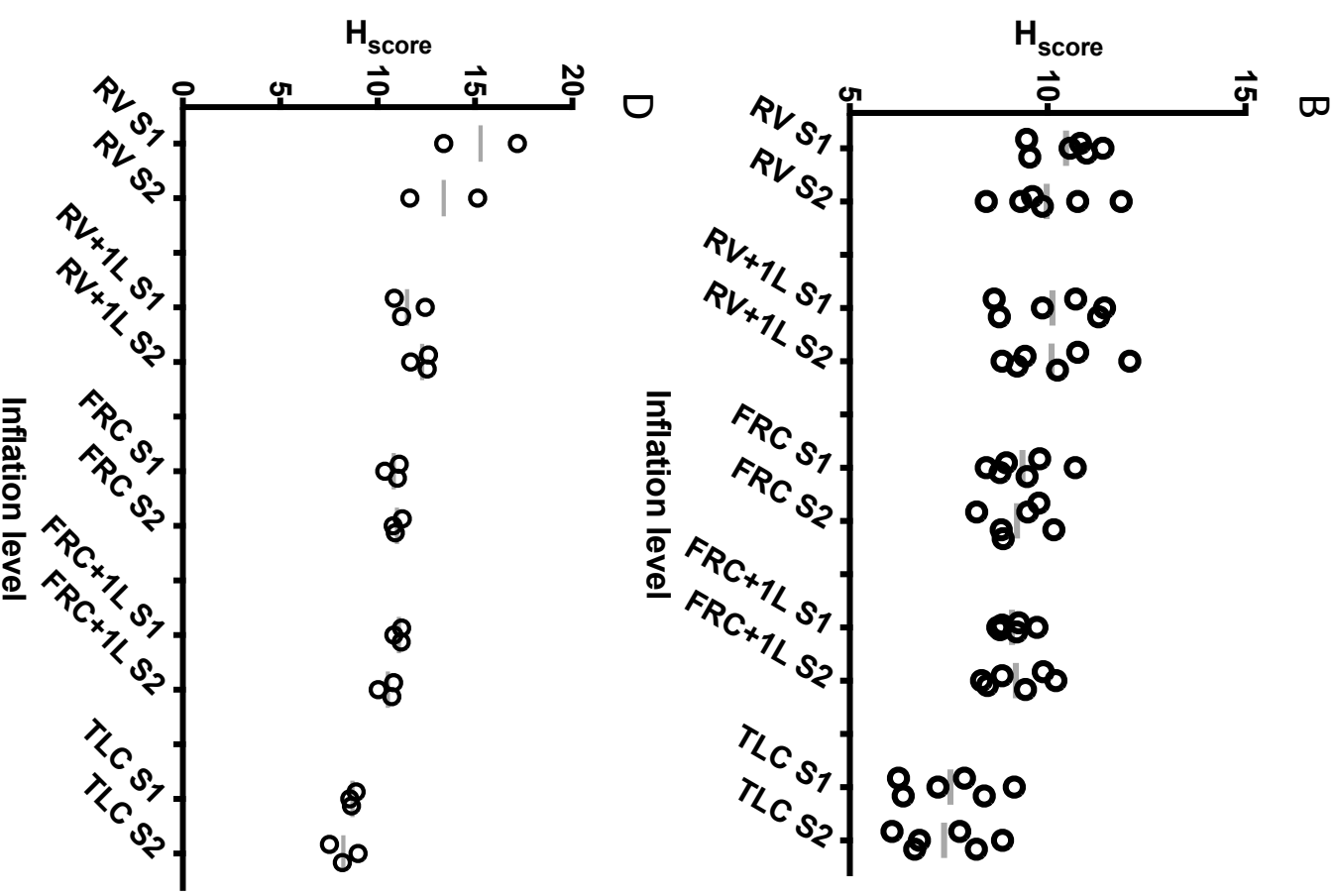
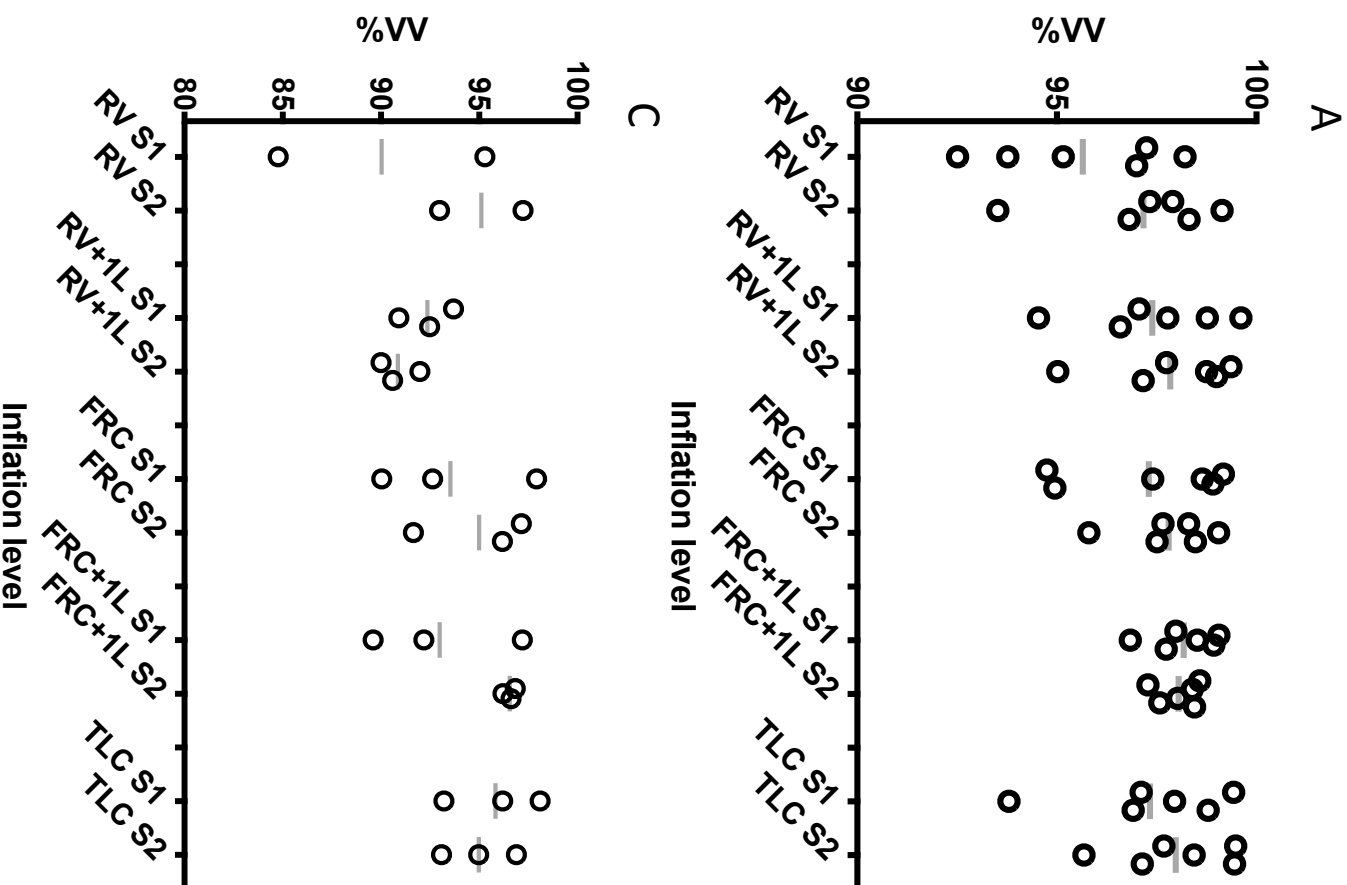


V2  $^3\text{He}$   
images



V2  $^{129}\text{Xe}$   
images





HP gas  
ventilation-  
weighted image

Heterogeneity  
map

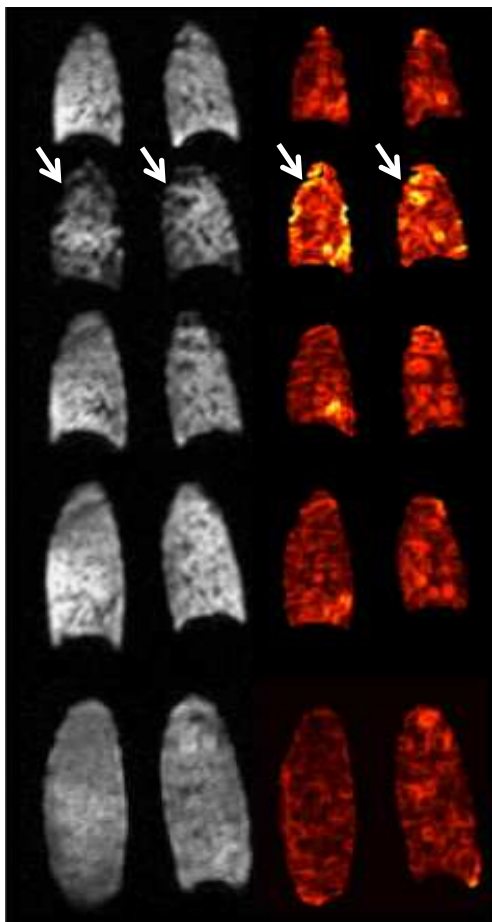
RV

RV+1L

FRC

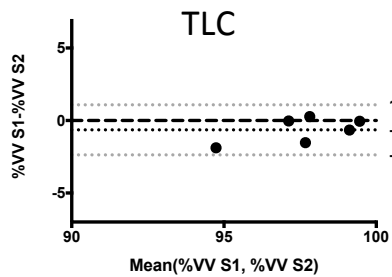
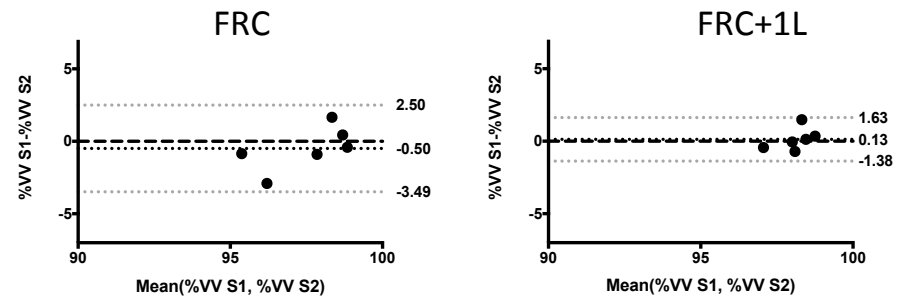
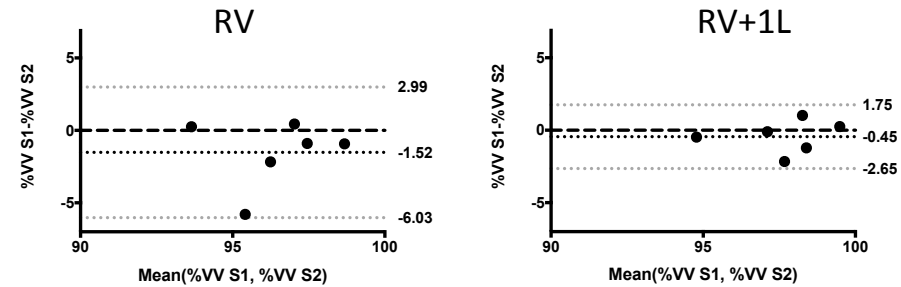
FRC+1L

TLC

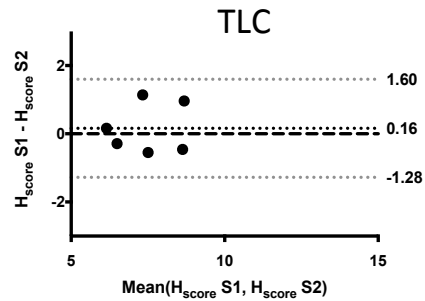
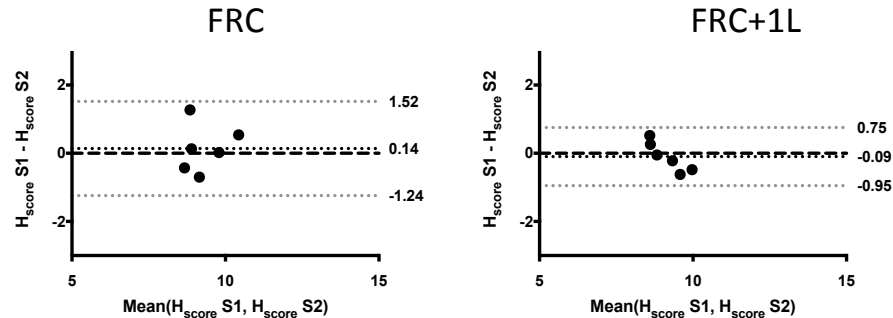
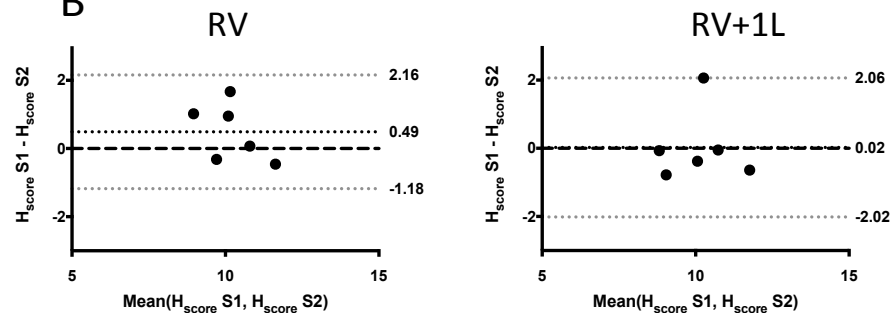


Hscore

A

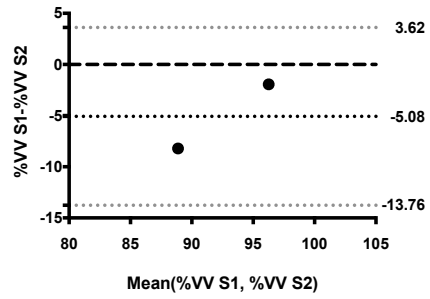


B

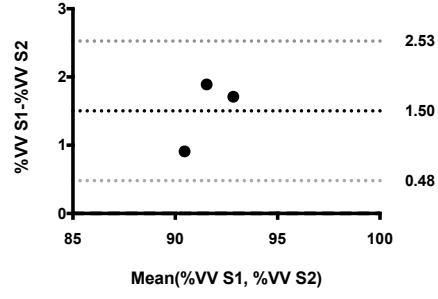


**A**

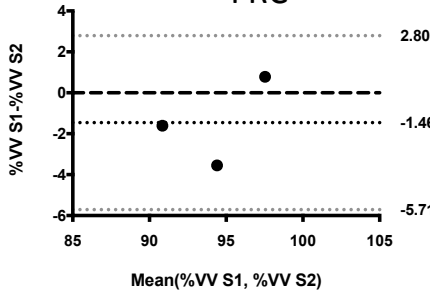
RV



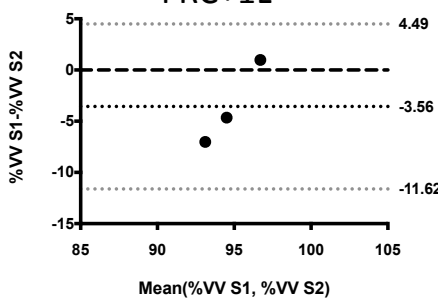
RV+1L



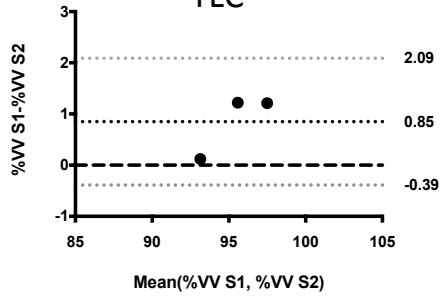
FRC



FRC+1L

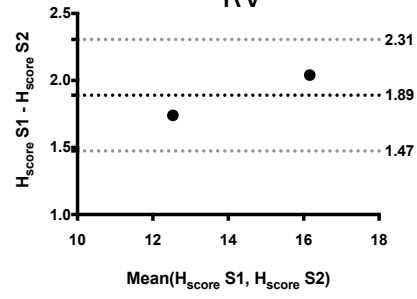


TLC

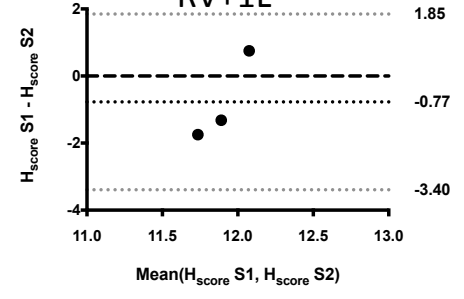


**B**

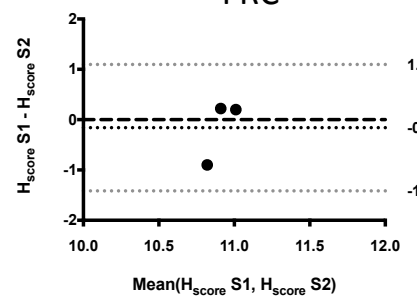
RV



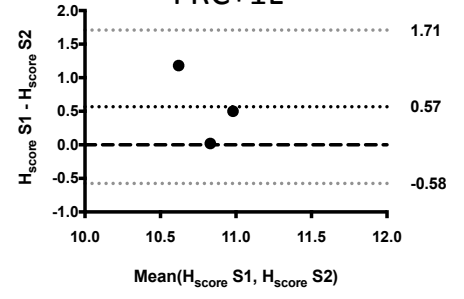
RV+1L



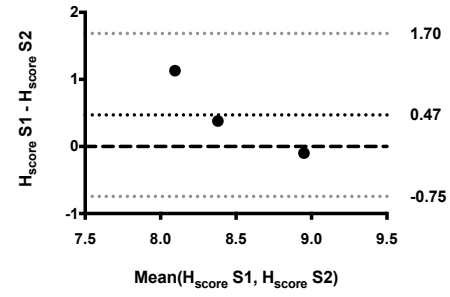
FRC



FRC+1L



TLC





• RV      ▲ FRC  
■ RV+1L    ◆ FRC+1L  
\* TLC

